CONVERGENCE OF FILTERED SPHERICAL HARMONIC EQUATIONS FOR RADIATION TRANSPORT *

MARTIN FRANK†, CORY HAUCK‡, AND KERSTIN KÜPPER§

Abstract. We analyze the global convergence properties of the filtered spherical harmonic (FP_N) equations for radiation transport. The well-known spherical harmonic (P_N) equations are a spectral method (in angle) for the radiation transport equation and are known to suffer from Gibbs phenomena around discontinuities. The filtered equations include additional terms to address this issue that are derived via a spectral filtering procedure. We show explicitly how the global L^2 convergence rate (in space and angle) of the spectral method to the solution of the transport equation depends on the smoothness of the solution (in angle only) and on the order of the filter. The results are confirmed by numerical experiments. Numerical tests have been implemented in MATLAB and are available online.

1. Introduction. The purpose of this paper is to analyze the global convergence properties of the filtered spherical harmonic (FP_N) equations [27, 34], a system of hyperbolic balance laws that are used to model radiation transport. These equations are a modification of the well-known spherical harmonic (P_N) system [10,24,33], which is derived via a global spectral approximation in angle of the solution to the radiation transport equation. Like any spectral approximation, the P_N system may suffer from Gibbs phenomena around discontinuities that can lead to highly oscillatory behavior and even negative particle concentrations [7]. This fact is considered one of the major drawbacks of the P_N method. The natural way to address deficiencies in the P_N equations is to modify the spectral approximation; indeed, the P_N approximation is just a linear combination of spherical harmonics and is not guaranteed to be positive.

There are a variety of nonlinear approximations that ensure positivity. For example, entropy-based methods [13,30] yield, among other things, positive approximations for low-order expansions and have produced promising results in several applications [4, 14, 16, 25, 32, 39]. However, the implementation of high-order expansions is computationally expensive because of the complicated relationship between the coefficients and the moments of the expansion [1, 2].[1] Positivity can also be enforced directly through inequality constraints [19] or by penalty methods [15]. However, these approaches are also computationally expensive when compared to the P_N equations. In addition, all of these methods still suffer from Gibbs-like phenomena around discontinuities.

Another method that uses a positive approximation of the transport solution is the quadrature method of moments (QMOM) [29]. Although the theoretical properties of

*The submitted manuscript has been authored, in part, by a contractor of the U.S. Government under Contract No. DE-AC05-00OR22725. Accordingly, the U.S. Government retains a nonexclusive, royalty-free license to publish or reproduce the published form of this contribution, or allow others to do so, for U.S. Government purposes. This material is based, in part, upon work supported by the National Science Foundation under Grant No. 1217170 and by NSF RNMS (KI-Net) Grant No. 11-07291

† Department of Mathematics & Center for Computational Engineering Science, Schinkelstrasse 2, D-52062 Aachen, Germany (frank@mathcces.rwth-aachen.de).

‡ Applied and Computational Mathematics Group, Oak Ridge National Laboratory, P.O. Box 2008 MS6164, Oak Ridge, TN 37831-6164 and Department of Mathematics, University of Tennessee, Knoxville, TN 37996-1320 (hauckc@ornl.gov).

§ Department of Mathematics & Center for Computational Engineering Science, Schinkelstrasse 2, D-52062 Aachen, Germany (kuepper@mathcces.rwth-aachen.de).

[1] For a standard spectral method like the P_N equations, this relationship is linear and often diagonal.

this method are not well-understood, the solution algorithm is simple and relatively fast. There are several variations of QMOM. (See, for example, [26] and references therein.) One such variation, known as extended QMOM (EQMOM) has been used to simulate thermal radiative transfer in one-dimensional slab geometries [41]. However, its fidelity for multi-dimensional radiative transport problems has yet to be evaluated.

A very simple modification of the P_N method, which does not significantly increase the computational cost, is to dampen, or filter, the coefficients in the expansion. Filtering has been widely used in conjunction with spectral methods to handle instabilities and oscillations that often arise when simulating linear and nonlinear advection. There are many papers on filtering in the literature. We refer the interested reader to [5, 17, 22] for analysis, further background, and a host of additional references.

Filters were first applied to the P_N equations in [27, 28]. There it was observed that the filtering process suppresses Gibbs phenomena in the spectral approximation of the angular variable, leading to significantly improved results for several challenging, multi-dimensional problems in radiative transfer. In its original form, the filter was applied after each stage of a time integration scheme; unfortunately, this approach is not consistent with any continuum equation in the limit of a vanishing time step. However in [34], the strength of the filter was made to depend on the time step in such a way as to give a modified system of equations in the continuum limit. This new system contains an additional artificial scattering operator that is analogous to the artificial viscosity induced by filtering methods for spatial discretizations of hyperbolic equations [5]. As with the original discrete approach, the filter strength is still an adjustable parameter. However, because of the consistent implementation, the parameter can be tuned once on a relatively coarse mesh and then held fixed under mesh refinement. In addition, the modified equations are more amenable to numerical analysis than the original filtering procedure is.

The filtering approach does have some drawbacks. Unlike the other methods discussed above, the filtered spectral approximation is not a projection, i.e., it is lossy. In addition, the approximation is not strictly positive. Finally, there is no optimal value for the filter strength; rather it may require adjustments for different problems. What's more, the "best value" of the filter strength depends on the local solution: suppressing oscillations in some regions causes a loss of accuracy in others. In spite of these drawbacks, the FP_N equations are a promising tool for simulating radiation transport due to their efficiency, overall accuracy, and simplicity.

In this paper, we analyze the global convergence properties of the FP_N equations derived in [34]. In particular, we show explicitly how the global L^2 convergence rate depends on the smoothness of the solution and the order of the filter. The analysis results are confirmed by numerical experiments. Such results are a helpful guide for practitioners who will use the equations for scientific simulation.

The remainder of the paper is organized as follows. In section 2, we introduce the filtered spherical harmonic equations. In section 3, we state and prove our main theorem, which gives the convergence rate of the filtered P_N method. Finally, several numerical tests are presented in section 4, to confirm the dependence of the convergence rate on the regularity of the solution and the order of the filter.

2. Background. In this section we introduce the transport equation, the spherical harmonics (P_N) equations, and the filtered spherical harmonic (FP_N) equations.

2.1. Radiative Transport. We consider the Cauchy problem

$$\partial_t \psi(t,x,\Omega) + \Omega \cdot \nabla_x \psi(t,x,\Omega) + \sigma_{\mathrm{a}}(x)\psi(t,x,\Omega) - (\mathcal{Q}\psi)(t,x,\Omega) = S(t,x,\Omega)\,, \quad \text{(2.1a)}$$

$$\psi(0,x,\Omega) = \psi_0(x,\Omega)\,, \quad \text{(2.1b)}$$

where the unknown $\psi(t,x,\Omega)$ gives the density of particles, with respect to the measure $d\Omega dx$, that at time $t \in \mathbb{R}$ are located at position $x \in \mathbb{R}^3$ and moving in the direction $\Omega \in \mathbb{S}^2$. The scattering operator $\mathcal{Q}$ describes the change in particle direction due to collisions with a fixed background medium:

$$(\mathcal{Q}\psi)(t,x,\Omega) = \sigma_{\mathrm{s}}(x) \int_{\mathbb{S}^2} g(x, \Omega\cdot\Omega')\psi(t,x,\Omega')d\Omega' - \psi(t,x,\Omega)\,, \quad (2.2)$$

where for each x, $g(x,\cdot)$ is a non-negative probability density on the interval $[-1,1]$. Thus $\mathcal{Q}$ is an integral operator in Ω, but local in x and t.

For each fixed x and t, $\mathcal{Q}$ is a self-adjoint, bounded linear operator from $L^2(\mathbb{S}^2)$ to itself. It has a nontrivial null space comprised of functions that are constant with respect to Ω. Orthogonal to the null space, $-\mathcal{Q}$ is coercive—that is, there exits a constant $c > 0$ such that

$$\int_{\mathbb{S}^2} h(-\mathcal{Q}h)d\Omega \geq c\|h\|^2_{L^2(\mathbb{S}^2)} \quad \text{for all } h \in [\mathrm{Null}(\mathcal{Q})]^{\perp}\,. \quad (2.3)$$

These properties are standard results in kinetic transport theory; their proofs can be found e.g. in [12, Chapter XXI] or in [11].

In what follows we use the abstract notation $\mathcal{T}\psi = S$ for (2.1a), where $\mathcal{T}$ denotes the linear integro-differential operator on the left-hand side. We also use angle brackets as a short-hand for angular integration over $\mathbb{S}^2$:

$$\langle\cdot\rangle = \int_{\mathbb{S}^2} (\cdot)\, d\Omega\,. \quad (2.4)$$

2.2. Spherical Harmonic ($\mathbf{P}_N$) Equations. The spherical harmonic (P_N) equations are derived from a spectral Galerkin discretization of the transport equation, using spherical harmonic functions as a basis. These functions and their properties are classical (see, for example, [3, 31]), but for completeness we briefly describe them here. We write

$$\Omega = (\Omega_1, \Omega_2, \Omega_3)^T = (\sqrt{1-\mu^2}\cos(\varphi), \sqrt{1-\mu^2}\sin(\varphi), \mu)^T\,, \quad (2.5)$$

where $\mu := \Omega_3 \in [-1,1]$ and $\varphi \in [0, 2\pi)$ is the angle between the x_1-axis and the projection of Ω onto the x_1-x_2 plane. Given integers $\ell \geq 0$ and $k \in [-\ell, \ell]$, the normalized, complex-valued spherical harmonic of degree ℓ and order k is expressed in terms of μ and φ as

$$Y_\ell^k(\Omega) = \sqrt{\frac{2\ell+1}{4\pi}\frac{(\ell-k)!}{(\ell+k)!}}e^{ik\varphi}P_\ell^k(\mu)\,, \quad (2.6)$$

where P_ℓ^k is an associated Legendre function. The primary motivation for using the spherical harmonics is that they form a complete set of eigenfunctions for $\mathcal{Q}$:

$$\mathcal{Q}Y_\ell^k = \sigma_{\mathrm{s}}(g_\ell - 1)Y_\ell^k\,, \quad \ell = 0,1,2,\ldots \text{ and } k = -\ell,\ldots,0,\ldots,\ell\,, \quad (2.7)$$

where $g_\ell = 2\pi \int_{-1}^{1} P_\ell g(\mu,\cdot)d\mu$ and P_ℓ is the degree ℓ Legendre polynomial with normalization $\int_{-1}^{1} P_\ell^2 d\mu = \frac{2}{2\ell+1}$. The eigenvalue relation (2.7) is derived by expanding the kernel g in Legendre polynomials and then applying the addition formula for spherical harmonics (see, for example, [23, Appendix A] or [24]), and it reduces the approximation of $\mathcal{Q}$ in the Galerkin method from an $O(N^2)$ to an $O(N)$ operation.

For convenience, we use the real-valued spherical harmonics which, up to a normalization factor, are the real and imaginary parts of each Y_ℓ^k:

$$m_\ell^k = \begin{cases} \frac{(-1)^k}{\sqrt{2}}(Y_\ell^k + (-1)^k Y_\ell^{-k}) \,, & k > 0 \,, \\ Y_\ell^0 \,, & k = 0 \,, \\ -\frac{(-1)^k i}{\sqrt{2}}(Y_\ell^{-k} - (-1)^k Y_\ell^k) \,, & k < 0 \,. \end{cases} \tag{2.8}$$

We collect the $n_\ell := 2\ell+1$ real-valued harmonics of degree ℓ together into a vector-valued function $\mathbf{m}_\ell$ and then for given N, set $\mathbf{m} = (\mathbf{m}_0, \mathbf{m}_1, \ldots, \mathbf{m}_N)$. In all, $\mathbf{m}$ has $n := \sum_{l=0}^{N} n_l = (N+1)^2$ components which form an orthonormal basis for the space

$$\mathbb{P}_N = \left\{ \sum_{\ell=0}^{N} \sum_{k=-\ell}^{\ell} c_\ell^k m_\ell^k : c_\ell^k \in \mathbb{R} \text{ for } 0 \le \ell \le N,\ |k| \le \ell \right\}. \tag{2.9}$$

Finally, the spherical harmonics fulfill a recursion relation of the form

$$\Omega_i \mathbf{m}_\ell = \mathbf{a}_{\ell+1}^{(i)} \mathbf{m}_{\ell+1} + \left(\mathbf{a}_{\ell-1}^{(i)}\right)^T \mathbf{m}_{\ell-1} \text{ , where } \mathbf{a}_\ell^{(i)} \in \mathbb{R}^{(2\ell-1)\times(2\ell+1)}. \tag{2.10}$$

More details, including exact expressions for the matrices $\mathbf{a}_\ell^{(i)}$, can be found in the appendix.

The P_N equations are derived by approximating ψ by a function $\psi_{\mathrm{P}_N} \in \mathbb{P}_N$:

$$\psi \approx \psi_{\mathrm{P}_N} \equiv \mathbf{m}^T \mathbf{u}_{\mathrm{P}_N} \,, \tag{2.11}$$

where $\mathbf{u}_{\mathrm{P}_N} : \mathbb{R} \times \mathbb{R}^3 \ni (t,x) \mapsto \mathbf{u}_{\mathrm{P}_N}(t,x) \in \mathbb{R}^n$ solves

$$\langle \mathbf{m}\mathcal{T}(\mathbf{m}^T \mathbf{u}_{\mathrm{P}_N}(t,x)\rangle = \mathbf{s}(t,x) \,, \qquad (t,x) \in (0,\infty) \times \mathbb{R}^3 \,, \tag{2.12a}$$

$$\mathbf{u}_{\mathrm{P}_N}(0,x) = \langle \mathbf{m}\psi_0(x,\cdot)\rangle \,, \qquad x \in \mathbb{R}^3 \,, \tag{2.12b}$$

and $\mathbf{s} := \langle \mathbf{m}S\rangle$. Using (2.1a), the system (2.12a) can be written more explicitly as

$$\partial_t \mathbf{u}_{\mathrm{P}_N} + \mathbf{A} \cdot \nabla_x \mathbf{u}_{\mathrm{P}_N} + \sigma_{\mathrm{a}} \mathbf{u}_{\mathrm{P}_N} - \sigma_{\mathrm{s}} \mathbf{G} \mathbf{u}_{\mathrm{P}_N} = \mathbf{s}, \tag{2.13}$$

where $\mathbf{A} := \langle \mathbf{m}\mathbf{m}^T \Omega\rangle$, $\mathbf{G}$ is diagonal with components $G_{(\ell,k),(\ell,k)} = g_\ell - 1$, and we have used the fact that $\langle \mathbf{m}\mathbf{m}^T\rangle = I$. The inner product between $\mathbf{A}$ and the gradient is understood as

$$\mathbf{A} \cdot \nabla_x \equiv \sum_{i=1}^{3} \mathbf{A}_i \partial_{x_i}. \tag{2.14}$$

where $\mathbf{A}_i = \langle \mathbf{m}\mathbf{m}^T \Omega_i\rangle$. Moreover, due to the recursion relation (2.10), the structure of the matrices $\mathbf{A}_i$ is very specific:

$$\mathbf{A}_i = \begin{bmatrix} 0 & \mathbf{a}_1^{(i)} & & \\ \left(\mathbf{a}_1^{(i)}\right)^T & 0 & \mathbf{a}_2^{(i)} & \\ & \ddots & \ddots & \ddots \\ & & \left(\mathbf{a}_{N+1}^{(i)}\right)^T & 0 \end{bmatrix}. \tag{2.15}$$

2.3. Filtered Spherical Harmonic (FP$_N$) Equations. The filtered spherical harmonics (FP$_N$) method was originally introduced as a modification in a time integration scheme [27,28]. After each time step, the spherical harmonic expansion is filtered, using for example a spectral spline filter. It was later shown [34] that if the filtering function is raised to some strength parameter depending on the time step Δt, then the filtering procedure is consistent with a set of modified equations. Before presenting these equations, we first introduce the definition of a filter:

DEFINITION 1. *A filter of order α is a real-valued function $f \in C^{\alpha}(\mathbb{R}^+)$ that satisfies*

$$\text{(i) } f(0) = 1\,, \quad \text{(ii) } f^{(a)}(0) = 0, \text{ for } a = 1, \dots, \alpha - 1\,, \quad \text{(iii) } f^{(\alpha)}(0) \neq 0. \tag{2.16}$$

REMARK 1. *There are several slightly different definitions of a filter in the literature [5, 9, 21, 22, 34, 40]. In [22] a filter of order α is a real-valued, even function $f \in C^{\alpha-1}(\mathbb{R})$ that, in addition to conditions (i) and (ii) above, satisfies*

$$\text{(iv) } f(\eta) = 0 \text{ for } |\eta| \geq 1 \quad \text{and} \quad \text{(v) } f^{(a)}(1) = 0 \text{ for } a = 0, 1, \dots, \alpha - 1. \tag{2.17}$$

Conditions (i) and (ii) are essential to every filter, but the other requirements may vary slightly. Commonly used filters are additionally strictly monotone decreasing on the interval $[0, 1]$ and smoother than required. At the same time, some filters do not satisfy conditions (iv) or (v). For example, neither the fourth order spherical spline filter, $f(\eta) = \frac{1}{\eta^4+1}$, nor the exponential filter of order α:

$$f(\eta) = \exp(c\eta^{\alpha}) \quad \text{with} \quad c = \log(\varepsilon_M), \tag{2.18}$$

where ε_M is the machine accuracy, satisfy these conditions. Since filtering functions like the exponential filter are suitable for our purposes, we neglect conditions (iv) and (v) in the above definition. Condition (iii) has been added so that the filter order becomes a unique property.

ASSUMPTION 1. *In what follows, we make the additional technical assumption that the filter f satisfies*

$$\text{(vi) } f(\eta) \geq C(1 - \eta)^k\,, \quad \eta \in [\eta_0, 1] \tag{2.19}$$

for some $k \geq 0$, some constant C, and some $\eta_0 \in (0, 1)$. This condition will be used in the proof of Theorem 3.3.

REMARK 2. *Filters in the sense of Definition 1 that satisfy Assumption 1 include the exponential filter (which we use in computations) or any C^{α}-function that satisfies conditions (i)-(v) above.*

In [34], the truncated filtered spherical harmonic expansion of a function Φ with expansion coefficients Φ_ℓ^k is given by

$$\sum_{\ell=0}^{N} \sum_{k=-\ell}^{\ell} \left(f\left(\tfrac{\ell}{N+1}\right) \right)^{\sigma_{\mathrm{f}} \Delta t} \Phi_\ell^k m_\ell^k, \tag{2.20}$$

where f is the filter and $\sigma_{\mathrm{f}} \Delta t$ is a filter strength that is tuned by the selection of the filtering cross-section σ_{f} or, equivalently, the filter effective opacity

$$f_{\mathrm{eff}} = \sigma_{\mathrm{f}} \log\left(f\left(\tfrac{N}{N+1} \right) \right)\,. \tag{2.21}$$

The dependence of the filter strength on Δt allows one to express, in the formal limit $\Delta t \to 0$, the filtered spherical harmonic (FP$_N$) equations in the following continuum form [34]:

$$\partial_t \mathbf{u}_{\mathrm{FP}_N} + \mathbf{A} \cdot \nabla_x \mathbf{u}_{\mathrm{FP}_N} + \sigma_{\mathrm{a}} \mathbf{u}_{\mathrm{FP}_N} - \sigma_{\mathrm{s}} \mathbf{G} \mathbf{u}_{\mathrm{FP}_N} - \sigma_{\mathrm{f}} \mathbf{G}_{\mathrm{f}} \mathbf{u}_{\mathrm{FP}_N} = \mathbf{s}, \tag{2.22}$$

where $\mathbf{G}_{\mathrm{f}}$ is a diagonal matrix with components $(\mathbf{G}_{\mathrm{f}})_{(\ell,k),(\ell,k)} = \log\left(f\left(\frac{\ell}{N+1}\right)\right)$. Back in the abstract notation, (2.22) can be written as

$$\langle \mathbf{m} \mathcal{T}(\psi_{\mathrm{FP}_N}) \rangle - \langle \mathbf{m} \mathcal{Q}_{\mathrm{f}}(\psi_{\mathrm{FP}_N}) \rangle = \mathbf{s}, \tag{2.23}$$

where the operator $\mathcal{Q}_{\mathrm{f}}$ depends on $\mathbf{G}_{\mathrm{f}}$:

$$\mathcal{Q}_{\mathrm{f}}(\Phi) = \sigma_{\mathrm{f}} \mathbf{m}^T \mathbf{G}_{\mathrm{f}} \langle \mathbf{m} \Phi \rangle. \tag{2.24}$$

In a way, the FP$_N$ equations can be viewed as a Galerkin method for the transport equation (2.1a), but with an additional scattering operator that depends on N.

3. Error Estimate. In this section we analyze the L^2 convergence of the FP$_N$ method. This will require assumptions on the regularity of the transport solution.

3.1. Preliminaries. We begin by defining the spaces and operators that will be used in the analysis, using Φ and $\mathbf{u}$ to denote generic scalar and vector-valued functions.

- For any nonnegative integer q, $H^q(\mathbb{S}^2)$ denotes the Sobolev space on the unit sphere with norm

$$\|\Phi\|_{H^q(\mathbb{S}^2)} := \left(\sum_{|\alpha| \le q} \int_{\mathbb{S}^2} |D^\alpha \Phi(\Omega)|^2 d\Omega \right)^{1/2}. \tag{3.1}$$

  where the sum is over integer multi-indices α and the case $q = 0$ recovers the regular L^2 norm on $\mathbb{S}^2$. An equivalent weighted L^2 norm can be derived using the Beltrami (surface Laplacian) operator

$$\mathcal{L} = \frac{\partial}{\partial \mu} \left((1-\mu^2) \frac{\partial}{\partial \mu} \right) + \frac{1}{1-\mu^2} \frac{\partial^2}{\partial \varphi^2}, \tag{3.2}$$

  for which the spherical harmonics are also eigenfunctions:

$$\mathcal{L} m_\ell^k = -\lambda_\ell m_\ell^k, \quad \lambda_\ell = \ell(\ell+1). \tag{3.3}$$

  Therefore, the expansion coefficients $\Phi_\ell^k := \langle m_\ell^k \Phi \rangle$ of any function $\Phi \in H^{2q}(\mathbb{S}^2)$ satisfy

$$\Phi_\ell^k = \langle m_\ell^k \Phi \rangle = \frac{1}{(-\lambda_\ell)^q} \langle (\mathcal{L}^q m_\ell^k) \Phi \rangle = \frac{1}{(-\lambda_\ell)^q} \langle m_\ell^k \mathcal{L}^q \Phi \rangle, \tag{3.4}$$

  where the last equality in (3.4) follows from the differentiability of Φ and the fact that the Beltrami operator is self-adjoint. Therefore

$$\Phi \mapsto \left(\sum_{\ell=0}^{\infty} \sum_{k=-\ell}^{\ell} \ell^q (\ell+1)^q |\Phi_l^k|^2 \right)^{1/2} = \left(\sum_{\ell=0}^{\infty} \ell^q (\ell+1)^q \sum_{k=-\ell}^{\ell} |\Phi_l^k|^2 \right)^{1/2} \tag{3.5}$$

  defines an equivalent norm on $H^q(\mathbb{S}^2)$ that can then be extended to non-integer values of q [17, p. 317]. This norm will be used in the proofs of Theorems 3.3 and 3.4.

- For vectors $\mathbf{u} \in \mathbb{R}^n$ we define the Euclidean norm in the usual way: $\|\mathbf{u}\|_{\mathbb{R}^n} = \sqrt{\mathbf{u}^T\mathbf{u}}$. Since $\langle \mathbf{m}\mathbf{m}^T \rangle = I$, it follows that $\|\mathbf{m}^T\mathbf{u}\|_{L^2(\mathbb{S}^2)} = \|\mathbf{u}\|_{\mathbb{R}^n}$.
- For functions of space and angle, we define the space $L^2(\mathbb{R}^3; H^q(\mathbb{S}^2))$ by the norm

$$\|\Phi\|_{L^2(\mathbb{R}^3;H^q(\mathbb{S}^2))} := \left(\sum_{|\alpha|\le q} \int_{\mathbb{R}^3} \int_{\mathbb{S}^2} |D^\alpha \Phi(\Omega)|^2 d\Omega dx \right)^{1/2}. \tag{3.6}$$

For vector-valued functions of space, we define $L^2(\mathbb{R}^3; \mathbb{R}^n)$ by

$$\|\mathbf{u}\|_{L^2(\mathbb{R}^3;\mathbb{R}^n)} := \left(\int_{\mathbb{R}^3} \mathbf{u}(x)^T \mathbf{u}(x) dx \right)^{1/2}. \tag{3.7}$$

- Finally, we add time dependence. We define the space $C^0([0,T]; L^2(\mathbb{R}^3; H^q(\mathbb{S}^2)))$ by

$$\|\Phi\|_{C^0([0,T];L^2(\mathbb{R}^3;H^q(\mathbb{S}^2)))} := \sup_{t\in[0,T]} \left(\sum_{|\alpha|\le q} \int_{\mathbb{R}^3} \int_{\mathbb{S}^2} |D^\alpha \Phi(t,x,\Omega)|^2 d\Omega dx \right)^{1/2} \tag{3.8}$$

and $C^0([0,T]; L^2(\mathbb{R}^3; \mathbb{R}^n))$ by

$$\|\mathbf{u}\|_{C^0([0,T];L^2(\mathbb{R}^3;\mathbb{R}^n))} := \sup_{t\in[0,T]} \left(\int_{\mathbb{R}^3} \mathbf{u}(t,x)^T \mathbf{u}(t,x) dx \right)^{1/2}. \tag{3.9}$$

- The mapping

$$\mathcal{P}_N \Phi = \mathbf{m}^T \langle \mathbf{m}\mathbf{m}^T \rangle^{-1} \langle \mathbf{m}\Phi \rangle = \mathbf{m}^T \langle \mathbf{m}\Phi \rangle \tag{3.10}$$

is the L^2-orthogonal projection of a generic function $\Phi \in L^2(\mathbb{S}^2)$ onto $\mathbb{P}_N$. For any non-negative integer ℓ,

$$(\mathcal{P}_\ell - \mathcal{P}_{\ell-1})\Phi = \mathbf{m}_\ell^T \langle \mathbf{m}_\ell \mathbf{m}_\ell^T \rangle^{-1} \langle \mathbf{m}_\ell \Phi \rangle = \mathbf{m}_\ell^T \langle \mathbf{m}_\ell \Phi \rangle \tag{3.11}$$

is the L^2-orthogonal projection of Φ onto the space of homogeneous polynomials in Ω of degree ℓ. It is easy to show that

$$\|\langle \mathbf{m}_\ell \Phi \rangle\|_{\mathbb{R}^{n_\ell}} \equiv \|(\mathcal{P}_\ell - \mathcal{P}_{\ell-1})\Phi\|_{L^2(\mathbb{S}^2)} \le \|(\mathcal{I} - \mathcal{P}_\ell)\Phi\|_{L^2(\mathbb{S}^2)} \tag{3.12}$$

and the equivalent H^q norm in (3.5) is equal to $\sum_{\ell=0}^\infty \ell^q(\ell+1)^q \|\langle \mathbf{m}_\ell \Phi \rangle\|^2_{\mathbb{R}^{n_\ell}}$.

A standard existence and uniqueness result for the transport equation is
Theorem 3.1 ([12, Theorem XXI.2.3]). *Let*

$$\sigma_{\mathrm{s}}, \sigma_{\mathrm{a}} \in L^\infty(\mathbb{R}^3) \textit{ with } \sigma_{\mathrm{s}}, \sigma_{\mathrm{a}} \ge 0. \tag{3.13}$$

Let the initial condition ψ_0 be such that

$$\psi_0 \in L^2(\mathbb{R}^3; L^2(\mathbb{S}^2)) \quad \textit{and} \quad \Omega \cdot \nabla_x \psi_0 \in L^2(\mathbb{R}^3; L^2(\mathbb{S}^2)). \tag{3.14}$$

Furthermore, let the source S satisfy

$$S \in C^1([0,T]; L^2(\mathbb{R}^3; L^2(\mathbb{S}^2))). \tag{3.15}$$

Then there exists a unique solution that satisfies

$$u \in C^1([0,T];L^2(\mathbb{R}^3;L^2(\mathbb{S}^2))) \quad \textit{and} \quad \Omega\cdot\nabla_x\psi \in C^0([0,T];L^2(\mathbb{R}^3;L^2(\mathbb{S}^2))). \quad (3.16)$$

REMARK 3. *The assumptions of the Theorem can be weakened to allow for initial conditions that are not in the domain of the advection operator $\Omega\cdot\nabla_x$. Then there exists a C^0 solution. However, the convergence results below require estimates on the spatial gradient of ψ and additional regularity in angle. As Theorem 3.1 is a semigroup result, this could be achieved by additional regularity in the initial condition, see e.g. [6, Theorem 7.5]. In all our numerical examples, the initial condition is either zero or smooth.*

The FP_N equations are a symmetric hyperbolic system. Thus if the initial value $\mathbf{u}_{\mathrm{FP}_N}(0,\cdot) \in L^2(\mathbb{R}^3;\mathbb{R}^n)$, then a straight-forward Fourier analysis (see [38, Chapter 3]) shows that there is a unique solution $\mathbf{u}_{\mathrm{P}_N} \in C^0([0,T];L^2(\mathbb{R}^3;\mathbb{R}^n))$ and that, in the absence of a source, $\|\mathbf{u}_{\mathrm{FP}_N}\|_{L^2(\mathbb{R}^3;\mathbb{R}^n)}$ is bounded uniformly in time by the initial data. However, with the assumptions of Theorem 3.1, more can be said.

THEOREM 3.2. *Let $\mathbf{u}_{FP_N}(0,x) = \langle \mathbf{m}\psi_0\rangle$ and $\mathbf{s} = \langle \mathbf{m}S\rangle$, where ψ_0 and S satisfy* (3.14) *and* (3.15)*, respectively. Then there exists a unique solution that satisfies*

$$\mathbf{u}_{FP_N} \in C^1([0,T];L^2(\mathbb{R}^3;\mathbb{R}^n)) \quad \textit{and} \quad \mathbf{A}\cdot\nabla_x\mathbf{u}_{FP_N} \in C^0([0,T];L^2(\mathbb{R}^3;\mathbb{R}^n)). \quad (3.17)$$

This result follows from standard semigroup theory (see, e.g., [6, Theorem 7.4]). The regularity provided by (3.17) is sufficient for the analysis that follows.

3.2. Main Result. We now state and prove the main convergence result.

THEOREM 3.3. *Assume the transport solution ψ satisfies the additional regularity conditions*

$$\psi \in C^0([0,T];L^2(\mathbb{R}^3;H^q(\mathbb{S}^2))) \quad \textit{and} \quad \partial_{x_i}\psi \in C^0([0,T];L^2(\mathbb{R}^3;H^r(\mathbb{S}^2)))\,, \quad (3.18)$$

for each $i \in \{1,2,3\}$, where r and q are positive constants. Let $\psi_{FP_N} = \mathbf{m}^T\mathbf{u}_{FP_N}$ be the reconstructed solution to (2.23)*. Then for any $t \in [0,T]$,*

$$\begin{aligned}&\|\psi(t,\cdot,\cdot) - \psi_{FP_N}(t,\cdot,\cdot)\|_{L^2(\mathbb{R}^3;L^2(\mathbb{S}^2))} \le \|\psi(t,\cdot,\cdot) - \mathcal{P}_N\psi(t,\cdot,\cdot)\|_{L^2(\mathbb{R}^3;L^2(\mathbb{S}^2))}\\ &+ t\left\{\|\mathbf{a}_{N+1}\cdot\nabla_x\langle\mathbf{m}_{N+1}\psi\rangle\|_{C^0([0,T];L^2(\mathbb{R}^3;\mathbb{R}^{2N+1}))} + \sigma_{\mathrm{f}}\|\mathbf{G}_{\mathrm{f}}\langle\mathbf{m}\psi\rangle\|_{C^0([0,T];L^2(\mathbb{R}^3;\mathbb{R}^n))}\right\}\,,\end{aligned} \quad (3.19)$$

and as $N\to\infty$, we have the following rates:[2]

$$\|\psi(t,\cdot,\cdot) - \mathcal{P}_N\psi(t,\cdot,\cdot)\|_{L^2(\mathbb{R}^3;L^2(\mathbb{S}^2))} \le CN^{-q}\,, \quad (3.20a)$$

$$\|\mathbf{a}_{N+1}\cdot\nabla_x\langle\mathbf{m}_{N+1}\psi\rangle\|_{C^0([0,T];L^2(\mathbb{R}^3;\mathbb{R}^{2N+1}))} \le CN^{-r}\,, \quad (3.20b)$$

$$\|\mathbf{G}_{\mathrm{f}}\langle\mathbf{m}\psi\rangle\|_{C^0([0,T];L^2(\mathbb{R}^3;\mathbb{R}^n))} \le \begin{cases} CN^{-q+1/2}, & \alpha > q - \frac{1}{2} \\ CN^{-\alpha+\varepsilon}\ \forall\varepsilon > 0, & \alpha \le q - \frac{1}{2}\end{cases}. \quad (3.20c)$$

Theorem 3.3 allows one to predict the order of convergence of the FP_N solution as $N\to\infty$, depending on the order of the filter α and the smoothness of ψ. The term

[2]Throughout the paper, we use C as a generic positive constant.

in (3.20a) is the *projection error*. We refer to the term in (3.20b) as the *closure error*, and the term in (3.20c) as the *filter error*.

The remainder of this section is dedicated to proving Theorem 3.3. The strategy is a Galerkin-type estimate similar to [35]. As is standard, we split the total error into the projection error and a remainder that is an element of $\mathbb{P}_N$:

$$\psi - \psi_{\mathrm{FP}_N} = (\psi - \mathcal{P}_N\psi) + \mathbf{m}^T\mathbf{r}, \tag{3.21}$$

where $\mathbf{r} = \langle \mathbf{m}(\mathcal{P}_N\psi - \psi_{\mathrm{FP}_N})\rangle = \langle \mathbf{m}^T\psi\rangle - \mathbf{u}_{\mathrm{FP}_N}$ inherits the regularity in (3.17). The first step is to control $\mathbf{r}$.

LEMMA 1. *Let ψ be the exact solution to* (2.1a) *and $\psi_{FP_N} = \mathbf{m}^T\mathbf{u}_{FP_N}$ be the solution to* (2.23). *Then for any $t \in [0,T]$, the residual vector $\mathbf{r}$ in* (3.21) *satisfies the estimate*

$$\begin{aligned}\|\mathbf{r}(t,\cdot)\|_{L^2(\mathbb{R}^3;\mathbb{R}^n)} \le t\big\{&\|\mathbf{a}_{N+1}\cdot\nabla_x\langle\mathbf{m}_{N+1}\psi(t,\cdot,\cdot)\rangle\|_{C^0([0,T];L^2(\mathbb{R}^3;\mathbb{R}^{2N+1}))}\\ &+\sigma_{\mathrm{f}}\|\mathbf{G}_{\mathrm{f}}\langle\mathbf{m}\psi(t,\cdot,\cdot)\rangle\|_{C^0([0,T];L^2(\mathbb{R}^3;\mathbb{R}^n))}\big\}.\end{aligned} \tag{3.22}$$

Proof. The proof is essentially a calculation. We apply $\mathcal{T}$ to (3.21), then multiply by $\mathbf{m}^T\mathbf{r}$ and integrate in angle. Since ψ is the exact transport solution, $\langle\mathbf{m}\mathcal{T}(\psi)\rangle = \mathbf{s}$. Combined with (2.23), this gives for the left-hand side of (3.21)

$$\langle\mathbf{m}^T\mathbf{r}\,\mathcal{T}(\psi-\psi_{\mathrm{FP}_N})\rangle = -\langle\mathbf{m}^T\mathbf{r}\,\mathcal{Q}_{\mathrm{f}}(\psi_{\mathrm{FP}_N})\rangle \tag{3.23a}$$
$$= -\langle\mathbf{m}^T\mathbf{r}\,\mathcal{Q}_{\mathrm{f}}(\mathcal{P}_N\psi)\rangle - \langle\mathbf{m}^T\mathbf{r}\,\mathcal{Q}_{\mathrm{f}}(\mathbf{m}^T\mathbf{r})\rangle \tag{3.23b}$$

Equating this to the result for the right-hand side, we find

$$\langle\mathbf{m}^T\mathbf{r}\mathcal{T}(\mathbf{m}^T\mathbf{r})\rangle - \langle\mathbf{m}^T\mathbf{r}\mathcal{Q}_{\mathrm{f}}(\mathbf{m}^T\mathbf{r})\rangle = -\langle\mathbf{m}^T\mathbf{r}\mathcal{T}(\psi-\mathcal{P}_N\psi)\rangle - \langle\mathbf{m}^T\mathbf{r}\mathcal{Q}_{\mathrm{f}}(\mathcal{P}_N\psi)\rangle. \tag{3.24}$$

The individual terms in (3.24) can be explicitly computed:

$$\langle\mathbf{m}^T\mathbf{r}\mathcal{T}(\mathbf{m}^T\mathbf{r})\rangle = \tfrac12\partial_t|\mathbf{r}|^2 + \tfrac12\nabla_x\cdot\langle\Omega|\mathbf{m}^T\mathbf{r}|^2\rangle + \sigma_{\mathrm{a}}|\mathbf{r}|^2 - \sigma_{\mathrm{s}}\mathbf{r}^T\mathbf{G}\mathbf{r} \tag{3.25a}$$
$$\langle\mathbf{m}^T\mathbf{r}\mathcal{Q}_{\mathrm{f}}(\mathbf{m}^T\mathbf{r})\rangle = \sigma_{\mathrm{f}}\mathbf{r}^T\mathbf{G}_{\mathrm{f}}\mathbf{r} \tag{3.25b}$$
$$\langle\mathbf{m}^T\mathbf{r}\mathcal{T}(\psi-\mathcal{P}_N\psi)\rangle = \langle\mathbf{m}^T\mathbf{r}\Omega\cdot\nabla_x(\psi-\mathcal{P}_N\psi)\rangle = \mathbf{r}_N^T\mathbf{a}_{N+1}\cdot\nabla_x\langle\mathbf{m}_{N+1}\psi\rangle \tag{3.25c}$$
$$\langle\mathbf{m}^T\mathbf{r}\mathcal{Q}_{\mathrm{f}}(\mathcal{P}_N\psi)\rangle = \sigma_{\mathrm{f}}\mathbf{r}^T\mathbf{G}_{\mathrm{f}}\langle\mathbf{m}\psi\rangle \tag{3.25d}$$

In (3.25c), we have used the notation defined in (2.14) and the recursion relation of the spherical harmonics in (2.10). After integration with respect to x we obtain

$$\tfrac12\partial_t\int_{\mathbb{R}^3}|\mathbf{r}|^2dx = -\int_{\mathbb{R}^3}\mathbf{r}_N^T\mathbf{a}_{N+1}\cdot\nabla_x\langle\mathbf{m}_{N+1}\psi\rangle dx - \sigma_{\mathrm{f}}\int_{\mathbb{R}^3}\mathbf{r}^T\mathbf{G}_f\langle\mathbf{m}\psi\rangle dx - \int_{\mathbb{R}^3}\mathbf{r}^T\mathbf{M}\mathbf{r}dx. \tag{3.26}$$

where $\mathbf{M} := \sigma_{\mathrm{a}}\mathbf{I} - \sigma_{\mathrm{s}}\mathbf{G} - \sigma_{\mathrm{f}}\mathbf{G}_{\mathrm{f}}$ is positive definite. This implies that

$$\partial_t\|\mathbf{r}\|_{L^2(\mathbb{R}^3;\mathbb{R}^n)} \le \|\mathbf{a}_{N+1}\cdot\nabla_x\langle\mathbf{m}_{N+1}\psi\rangle\|_{L^2(\mathbb{R}^3;\mathbb{R}^{2N+1})} + \sigma_{\mathrm{f}}\|\mathbf{G}_{\mathrm{f}}\langle\mathbf{m}\psi\rangle\|_{L^2(\mathbb{R}^3;\mathbb{R}^n)}, \tag{3.27}$$

and the result in (3.22) follows immediately. ◻

The next step is to prove the convergence rates in (3.20). The projection error rate in (3.20a) is well known (see, for example, [17,18]) and the result in (3.20b) follows a similar argument. We rederive these rates for completeness. Our convergence proof for the filter error follows the approach used in [20]. For all three cases, we utilize the equivalent H^q norm in (3.5) to simplify the presentation.

Projection error. Using equation (3.4) and Parseval's identity, the projection error satisfies

$$\begin{aligned}\|\psi(t,\cdot,\cdot)-\mathcal{P}_N\psi(t,\cdot,\cdot)\|^2_{L^2(\mathbb{R}^3;L^2(\mathbb{S}^2))} &= \int_{\mathbb{R}^3}\sum_{\ell=N+1}^{\infty}\sum_{k=-\ell}^{\ell}|\psi_\ell^k(t,x)|^2dx\\ &\le \frac{1}{(N+1)^{2q}}\int_{\mathbb{R}^3}\sum_{\ell=N+1}^{\infty}\sum_{k=-\ell}^{\ell}\ell^{2q}|\psi_\ell^k(t,x)|^2dx\\ &\le \frac{C}{N^{2q}}\|\psi(t,\cdot,\cdot)\|^2_{L^2(\mathbb{R}^3;H^q(\mathbb{S}^2))}.\end{aligned} \tag{3.28}$$

Closure error. We note first that for each $i\in\{1,2,3\}$, the scalar elements $\mathbf{a}^{(i)}_{N+1}$ are all bounded independently of N. Moreover, the number of nonzero components in any row or column is also bounded independently of N (see the appendix for more details). Thus $\|\mathbf{a}^{(i)}_{N+1}\|_2\le\|\mathbf{a}^{(i)}_{N+1}\|_1\|\mathbf{a}^{(i)}_{N+1}\|_\infty$ is uniformly bounded in N, and under the conditions of Theorem 3.3,

$$\begin{aligned}\|\mathbf{a}_{N+1}\cdot\nabla_x\langle\mathbf{m}_{N+1}\psi(t,\cdot,\cdot)\rangle\|^2_{L^2(\mathbb{R}^3;\mathbb{R}^{2N+1})} &\le C\sum_{i=1}^{3}\|\langle\mathbf{m}_{N+1}\partial_{x_i}\psi(t,\cdot,\cdot)\rangle\|^2_{L^2(\mathbb{R}^3;\mathbb{R}^{2N+3})}\\ &= C\sum_{i=1}^{3}\|(\mathcal{P}_{N+1}-\mathcal{P}_N)(\partial_{x_i}\psi(t,\cdot,\cdot))\|^2_{L^2(\mathbb{R}^3;L^2(\mathbb{S}^2))}\\ &\le C\sum_{i=1}^{3}\|(\mathcal{I}-\mathcal{P}_N)(\partial_{x_i}\psi(t,\cdot,\cdot))\|^2_{L^2(\mathbb{R}^3;L^2(\mathbb{S}^2))}\\ &\le \frac{C}{N^{2r}}\sum_{i=1}^{3}\|\partial_{x_i}\psi(t,\cdot,\cdot)\|^2_{L^2(\mathbb{R}^3;H^r(\mathbb{S}^2))}\,,\end{aligned} \tag{3.29}$$

where we have used (3.12) and the estimate of the projection error in (3.28), replacing q by r and ψ by $\partial_{x_i}\psi$. Taking the supremum over all $t\in[0,T]$ on both sides yields the desired rate.

Filter error. The filtering error satisfies

$$\begin{aligned}\|\mathbf{G}_{\mathrm{f}}\langle\mathbf{m}\psi(t,\cdot,\cdot)\rangle\|^2_{L^2(\mathbb{R}^3;\mathbb{R}^n)} &= \sum_{\ell=0}^{N}\log^2\left(f\left(\tfrac{\ell}{N+1}\right)\right)\|\langle\mathbf{m}_\ell\psi(t,\cdot,\cdot)\rangle\|^2_{L^2(\mathbb{R}^3;\mathbb{R}^{n_\ell})}\\ &= \sum_{\ell=1}^{N}\log^2\left(f\left(\tfrac{\ell}{N+1}\right)\right)\|(\mathcal{P}_\ell-\mathcal{P}_{\ell-1})\psi(t,\cdot,\cdot)\|^2_{L^2(\mathbb{R}^3;L^2(\mathbb{S}^2))}\\ &= C\sum_{\ell=1}^{N}\log^2\left(f\left(\tfrac{\ell}{N+1}\right)\right)\|(\mathcal{I}-\mathcal{P}_{\ell-1})\psi(t,\cdot,\cdot)\|^2_{L^2(\mathbb{R}^3;L^2(\mathbb{S}^2))}\\ &\le C\sum_{\ell=1}^{N}\log^2\left(f\left(\tfrac{\ell}{N+1}\right)\right)\frac{1}{\ell^{2q}}\|\psi(t,\cdot,\cdot)\|^2_{L^2(\mathbb{R}^3;H^q(\mathbb{S}^2))}\,.\end{aligned} \tag{3.30}$$

where we have again used (3.12) and the estimate of the projection error in (3.28). It remains to find an estimate for the sum in the last term of (3.30). We follow the strategy in [21], approximating this sum with a Riemann integral and then determining conditions under which the integral is bounded. For any $\theta \le 2q$,

$$\sum_{\ell=1}^{N} \log^2\left(f\left(\tfrac{\ell}{N+1}\right)\right)\frac{1}{\ell^{2q}} \le \frac{1}{(N+1)^{\theta-1}} \underbrace{\frac{1}{N+1}\sum_{\ell=1}^{N} \log^2\left(f\left(\tfrac{\ell}{N+1}\right)\right)\left(\tfrac{N+1}{\ell}\right)^{\theta}}_{=:\Sigma} . \tag{3.31}$$

The quantity Σ is a Riemann sum corresponding to the integral

$$\int_0^1 \log^2\left(f(\eta)\right)\eta^{-\theta} d\eta\,, \tag{3.32}$$

where the integrand is singular at $\eta = 0$ and $\eta = 1$. The singularity at $\eta = 1$ is because of the logarithm and is integrable under Assumption 1. The singularity at $\eta = 0$ is polynomial; for it to be integrable, one must impose additional conditions relating θ and the filter order α. A Taylor expansion of f around $\eta = 0$ yields

$$\log f(\eta) = \log\left(f(0) + \eta f'(0) + \ldots + \eta^{\alpha}\frac{f^{(\alpha)}(\xi)}{\alpha}\right) = \log\left(1 + \eta^{\alpha}\frac{f^{(\alpha)}(\xi)}{\alpha!}\right) \tag{3.33}$$

for some $\xi \in [0, \eta]$. Thus $\log f(\eta) \le C\eta^{\alpha}$ for η positive, but sufficiently small. As a consequence, the singularity at $\eta = 0$ will be integrable if and only if

$$\theta < 2\alpha + 1\,. \tag{3.34}$$

There are two cases:

Case 1: $\alpha > q - \frac{1}{2}$. In this case, convergence is limited by the regularity of ψ, and (3.34) is valid for all $\theta \le 2q$. In particular, for $\theta = 2q$, we obtain from (3.31) the estimate $\|\mathbf{G}_{\mathrm{f}}\langle \mathbf{m}\psi\rangle\|_{C^0([0,T];L^2(\mathbb{R}^3;\mathbb{R}^n))} \le CN^{-q+1/2}$.

Case 2: $\alpha \le q - \frac{1}{2}$. In this case, convergence is limited by the filter order, and (3.34) is valid only for $\theta = 2\alpha+1-\delta$, where $\delta > 0$ is arbitrary. We obtain from (3.31) the estimate $\|\mathbf{G}_{\mathrm{f}}\langle \mathbf{m}\psi\rangle\|_{C^0([0,T];L^2(\mathbb{R}^3;\mathbb{R}^n))} \le CN^{-\alpha+\varepsilon}$, where $\varepsilon = \delta/2$.

This completes the proof of Theorem 3.3.

3.3. A Sharper Estimate. The estimates of the closure filter errors in the previous section rely on the projection error estimate and the conservative bound of the projection $\mathcal{P}_{\ell} - \mathcal{P}_{\ell-1}$ that is expressed in (3.12). However, in the numerical results below, we observe faster decay rates that lead to sharper overall estimates.

Theorem 3.4. *In addition to the assumptions of Theorem 3.3, suppose that for all $\ell > 0$,*

$$\|\langle \mathbf{m}_{\ell}\psi\rangle\|_{C^0([0,T];L^2(\mathbb{R}^3;\mathbb{R}^{n_\ell}))} \le \frac{C}{\ell^{q+1/2}} \quad \text{and} \quad \|\mathbf{m}_{\ell}\partial_{x_i}\psi\|_{C^0([0,T];L^2(\mathbb{R}^3;\mathbb{R}^{n_\ell}))} \le \frac{C}{\ell^{r+1/2}}\,, \quad i \in \{1,2,3\}. \tag{3.35}$$

Then the rates in (3.20b) *and* (3.20c) *of Theorem 3.3 can be sharpened to*

$$\|\mathbf{a}_{N+1}\cdot\nabla_x\langle \mathbf{m}_{N+1}\psi\rangle\|_{C^0([0,T];L^2(\mathbb{R}^3;\mathbb{R}^{2N+1}))} \le CN^{-r-\frac{1}{2}} \tag{3.36}$$

$$\|\mathbf{G}_{\mathrm{f}}\langle \mathbf{m}\psi\rangle\|_{C^0([0,T];L^2(\mathbb{R}^3;\mathbb{R}^n))} \le \begin{cases} CN^{-q}, & \alpha > q \\ CN^{-\alpha+\varepsilon}\ \ \forall\varepsilon > 0, & \alpha \le q \end{cases} . \tag{3.37}$$

Proof. The proof is a trivial modification of the Theorem 3.3 proof. One simply needs to insert the bounds assumed in (3.35) into the appropriate place. ∎

REMARK 4. *The decay rates in* (3.35) *cannot be deduced from the Sobolev index alone. However, given sufficient smoothness, a subsequence of the expansion coefficients will always satisfy* (3.35).[3] *On the other hand, the decay rates in* (3.35) *imply that* $\psi \in C^0([0,T]; L^2(\mathbb{R}^3; H^{q_*}(\mathbb{S}^2)))$ *and* $\partial_{x_i}\psi \in C^0([0,T]; L^2(\mathbb{R}^3; H^{r_*}(\mathbb{S}^2)))$, *respectively, for any* $q_* < q$ *and* $r_* < r$.

4. Numerical Results. In this section, we compute the numerical rate of convergence for several test cases in two spatial dimensions (five dimensions total, including time). Here it is assumed that ψ is constant in x_3. Thus we fix x_3 and, in an abuse of notation, set $x = (x_1, x_2)$ and adapt the relevant definitions in Section 3.1 from $\mathbb{R}^3$ to $\mathbb{R}^2$. Beyond this, the results of Theorems 3.3 and 3.4 are unchanged.

The numerical calculations are performed using a modification of the code StaRMAP [37], which was originally designed for solving the P_N equations, but is easily modified for FP_N computations. The original code implements a fully-discrete, second-order, L^2-stable method that places even (u_ℓ^k with k even) and odd components (u_ℓ^k with k odd) on staggered grids and then uses central finite differences on one grid to approximate spatial gradients on the other. This is possible due to the specific coupling of the unknowns, which also enables a time stepping via a splitting of the sub-steps. In particular, the even components can be evaluated exactly if the odd components are assumed to be constant and vice-versa. Each time step Δt requires four substeps: updating the odd components by $\Delta t/2$, updating twice the even components ($\Delta t/2$ each time), then again updating the odd components by $\Delta t/2$. The size of the time step is related to the spatial resolution dx through the hyperbolic CFL condition $\Delta t = 0.99\Delta x/|\lambda_{\max}|$, where $|\lambda_{\max}|$ is the largest eigenvalue among the matrices $\mathbf{A}_i$ defined in (2.15).

To modify the code for the FP_N equations, we use (2.20), applying the filter f in each substep to the components that are updated in that substep. Filtering all components after a full solution time step with doubled filter strength yields similar results. The source code for all examples in this paper is available to the reader online [36].

We consider three test cases, each of which is designed to reveal one of the rates in Theorem 3.4. The *Gaussian test* has a smooth solution, so we expect a convergence rate determined by the filter order α. In the *lattice test*, we numerically determine the Sobolev indexes q and r of the true solution and its derivative; the convergence of the FP_N solution is determined by these indices. The *hemisphere test* has a solution that is smooth in space but discontinuous in angle; here the convergence order depends on the Sobolev index q.

For each test case, we compute both the P_N and FP_N solutions. The latter are computed using the exponential filter, cf. (2.18), using an effective filter opacity $f_{\text{eff}} = 10$ and several different filter orders: $\alpha \in \{2, 4, 8, 16\}$. The final time for

[3]For example, let the sequence $\{a_\ell\}_{\ell=0}^\infty$ be non-negative. Then the convergence of the series $\sum_{\ell=0}^\infty \ell^{2q} a_\ell^2$ does not imply $|a_\ell| \le C\ell^{-(q+1/2)}$; consider for instance the counterexample

$$a_\ell = \begin{cases} \ell^{-(q+1/4)}, & \text{for } \ell = 4^j\,, \quad j \in \{1, 2, \dots\}\,, \\ \frac{\ell^{-q}}{2^\ell}, & \text{otherwise}\,. \end{cases}$$

In fact, a_ℓ does not necessarily need to be bounded by $C\ell^{-(q+\gamma)}$ for any $\gamma > 0$. However, any subsequence of a_ℓ will always decay faster than $\ell^{-(q+1/2)}$.

Filter order	Gaussian		Lattice		Hemisphere	
	$\mathcal{E}_{33}^{65}$	$\mathcal{R}_{33}^{65}$	$\mathcal{E}_{17}^{33}$	$\mathcal{R}_{17}^{33}$	$\mathcal{E}_{17}^{33}$	$\mathcal{R}_{17}^{33}$
2	1.92	1.92	1.05	1.04	0.58	0.52
4	3.98	3.98	1.05	1.04	0.61	0.52
8	8.00	8.00	1.07	1.07	0.63	0.56
16	15.99	15.99	1.09	1.20	0.64	0.64
∞	18.32	17.43	1.02	0.95	0.65	0.96

Table 4.1: Approximate order of convergence for different filter orders and test cases. Spatial resolution 150×150 (Gaussian, hemisphere), 250×250 (lattice). Filter order of ∞ means that no filter is applied.

each problem is chosen so that the boundary does not affect the solution. Although Theorem 3.4 actually gives an estimate for the error in the $C^0([0,T])$-norm in time, we consider the error at a fixed final time. We however observe the expected rates.

We denote by E_N and R_N the norm of the total and projected error, respectively:

$$E_N = \|\psi - \psi_N\|_{L^2(\mathbb{R}^2;L^2(\mathbb{S}^2))} = \left(\sum_{\ell=0}^{\infty}\sum_{k=-\ell}^{\ell}\int_{\mathbb{R}^2}|\psi_\ell^k(x,t) - (\psi_N)_\ell^k(x,t)|^2 dx\right)^{\frac{1}{2}}, \quad (4.1)$$

$$R_N = \|\mathcal{P}\psi - \psi_N\|_{L^2(\mathbb{R}^2;L^2(\mathbb{S}^2))} = \left(\sum_{\ell=0}^{N}\sum_{k=-\ell}^{\ell}\int_{\mathbb{R}^2}|\psi_\ell^k(x,t) - (\psi_N)_\ell^k(x,t)|^2 dx\right)^{\frac{1}{2}}, \quad (4.2)$$

where ψ_N is either ψ_{FP_N} or ψ_{P_N}.[4] To estimate E_N and R_N we use the trapezoidal rule for the integrals and we approximate ψ by a $P_{N_{\mathrm{true}}}$ solution, with $N_{\mathrm{true}} \gg N$ sufficiently large. Thus the reference solution has a sharply higher angular resolution than ψ_{FP_N} and ψ_{P_N} but the same spatial resolution.

The error terms E_N and R_N are determined for different values of N, and we estimate the rate of convergence from two values N_1 and N_2 by

$$\mathcal{E}_{N_1}^{N_2} = -\frac{\log(E_{N_1}) - \log(E_{N_2})}{\log(N_1) - \log(N_2)} \quad \text{and} \quad \mathcal{R}_{N_1}^{N_2} = -\frac{\log(R_{N_1}) - \log(R_{N_2})}{\log(N_1) - \log(N_2)}. \quad (4.3)$$

The spatial resolution is chosen so that the space-time errors are negligibly small. To check this, we have performed a grid convergence study. A summary of the results is given in Table 4.1 and, with doubled spatial resolution, in Table 4.2.

According to Theorem 3.4, the order of E_N and R_N are given by

$$\begin{aligned} &\text{With filter:} && E_N \sim R_N = O(N^{-\min\{q, r+\frac{1}{2}, \alpha\}}). \\ &\text{Without filter:} && E_N = O(N^{-\min\{q, r+\frac{1}{2}\}}),\ R_N = O(N^{-(r+\frac{1}{2})}). \end{aligned} \quad (4.4)$$

In particular, both depend on the regularity of the solution, which is given by the values q and r. To obtain an estimate for these values, we estimate the order of decay for the moments of the solution and their differentials, cf. Lemma 1. Thus, we

[4] It can be shown that since ψ is independent of x_3, it is also invariant under the mapping $\Omega_3 \mapsto -\Omega_3$. As a consequence, moments with respect to m_ℓ^k vanish whenever $\ell + k$ is odd. The total number of nonzero moments that remain is $(N+1)(N+2)/2$.

Filter order	Gaussian		Lattice		Hemisphere	
	$\mathcal{E}_{33}^{65}$	$\mathcal{R}_{33}^{65}$	$\mathcal{E}_{17}^{33}$	$\mathcal{R}_{17}^{33}$	$\mathcal{E}_{17}^{33}$	$\mathcal{R}_{17}^{33}$
2	1.92	1.92	1.04	1.04	0.59	0.52
4	3.98	3.98	1.05	1.07	0.62	0.52
8	8.00	8.00	1.04	1.13	0.64	0.58
16	15.99	15.99	1.03	1.20	0.65	0.64
∞	17.87	16.94	0.99	0.96	0.66	0.96

Table 4.2: Approximate order of convergence for different filter orders and test cases. Spatial resolution 300×300 (Gaussian, hemisphere), 500×500 (lattice). Filter order of ∞ means that no filter is applied.

approximate

$$B_\ell := \|\langle \mathbf{m}_\ell \psi \rangle\|_{L^2(\mathbb{R}^2,\mathbb{R}^{n_\ell})} \quad \text{and} \quad D_\ell := \left(\sum_{i=1}^{3} \|\langle \mathbf{m}_\ell \partial_{x_i} \psi \rangle\|^2_{L^2(\mathbb{R}^2,\mathbb{R}^{n_\ell})} \right)^{1/2} \tag{4.5}$$

by using again the reference solution $P_{N_{\text{true}}}$ to estimate ψ and the trapezoidal rule to approximate the spatial integrals. As in (4.3), we use specific data points to define approximate decay rates

$$\mathcal{B}_{N_1}^{N_2} = -\frac{\log(B_{N_1}) - \log(B_{N_2})}{\log(N_1) - \log(N_2)} \quad \text{and} \quad \mathcal{D}_{N_1}^{N_2} = -\frac{\log(D_{N_1}) - \log(D_{N_2})}{\log(N_1) - \log(N_2)}. \tag{4.6}$$

Using (3.35), we approximate

$$q \approx \mathcal{B}_{N_1}^{N_2} - 0.5 \quad \text{and} \quad r \approx \mathcal{D}_{N_1}^{N_2} - 0.5\,. \tag{4.7}$$

4.1. Gaussian test. This first test case has smooth input data to show that the convergence order of the FP_N solution is bounded by the filter order α. All moments are initially zero, except the first:

$$u_\ell^k = \begin{cases} \frac{1}{4\pi \times 10^{-3}} \exp\left(-\frac{x^2+y^2}{4 \times 10^{-3}}\right), & k = \ell = 0 \\ 0\,, & \text{otherwise.} \end{cases} \tag{4.8}$$

The medium is purely scattering, with $\sigma_\mathrm{t} = \sigma_\mathrm{s} = 1$. The computational domain is $[-0.6, 0.6] \times [-0.6, 0.6]$ and the solution is computed on a 300×300 spatial grid (or 150×150 for Table 4.1) up to time $t = 0.4$. Errors are computed using a P_{99} reference solution. Since the initial condition is smooth, we expect spectral convergence for the P_N solution and a convergence order equal to the filter order for both E and R. This behavior is clearly confirmed in Table 4.3, where we observe that the convergence order increases until it reaches filter order or until the error reaches machine precision.

4.2. Lattice test. The lattice test was first proposed in [8]. It contains source terms and material cross-sections that are discontinuous in space. Due to the coupling of the spatial and the angular variable, this leads to a loss of regularity in the angular variable as well. Thus it is expected that the convergence order for E and R is determined by q and r.

For this problem, the computational domain is a 7×7 square that is divided into smaller squares of length one. There is an isotropic source in the middle of the domain

Filter order	$\mathcal{E}_3^5$	$\mathcal{E}_5^9$	$\mathcal{E}_9^{17}$	$\mathcal{E}_{17}^{33}$	$\mathcal{E}_{33}^{65}$	$\mathcal{R}_3^5$	$\mathcal{R}_5^9$	$\mathcal{R}_9^{17}$	$\mathcal{R}_{17}^{33}$	$\mathcal{R}_{33}^{65}$
2	0.47	0.84	1.33	1.73	1.92	0.03	0.52	1.28	1.73	1.92
4	0.76	1.57	2.89	3.79	3.98	0.36	1.05	2.68	3.78	3.98
8	1.01	2.13	4.93	7.61	8.00	1.14	1.68	4.30	7.54	8.00
16	1.06	2.40	6.15	13.61	15.99	1.29	2.63	5.53	12.95	15.99
∞	1.02	2.41	6.48	18.22	17.87	1.10	2.55	6.71	18.55	16.94

Table 4.3: Gauss test: Filter order of ∞ means that no filter is applied. The term $\mathcal{E}_{N_1}^{N_2}$ is the convergence rate when going from N_1 to N_2.

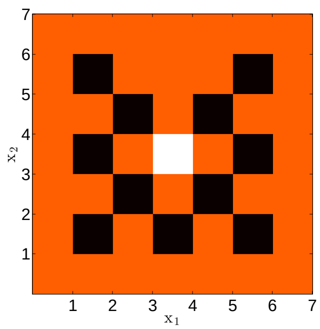

(a) Material coefficients

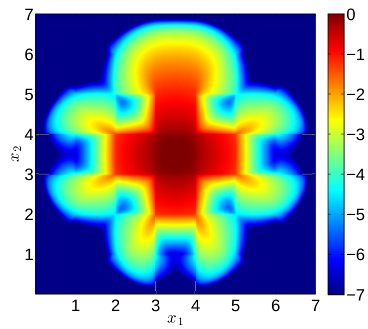

(b) $\phi = \langle\psi\rangle$ computed with P_{129}

Fig. 4.1: Lattice test. (a) Material coefficients: isotropic source (white square) $S = 1$; purely scattering $\sigma_t = \sigma_s = 1$ (orange and white squares); purely absorbing $\sigma_t = \sigma_a = 10$ (black squares). (b) Scalar flux $\phi = \langle\psi\rangle$ at $t = 2.8$ for P_{129}, computed with 500×500 grid points. The values are plotted in a logarithmic scale and limited to seven orders of magnitude.

and a mixture of purely scattering and purely absorbing squares surrounding it (c.f. Figure 4.1a). The P_N and FP_N solutions are computed on a 500×500 spatial grid (or 250×250 for Table 4.1) up to time $t = 2.8$. We use $N_{\text{true}} = 129$ (i.e. a system with more than 2.1×10^{10} degrees of freedom) to compute a reference solution and estimate convergence rates.

We estimate the decay rates of $\{B_\ell\}_{\ell=0}^\infty$ and $\{D_\ell\}_{\ell=0}^\infty$ which, due to the lack of regularity in the solution, converge very slowly. As a consequence numerical estimates of these values are not always reliable. In fact, we observe that they depend on the parity of both ℓ and the value of N_{true}. This behavior can be observed in Figure 4.2. To address it, we approximate B_ℓ and D_ℓ using both P_{128} and P_{129} numerical solutions and then determine a cutoff $\ell_{\max}$ so that the relative difference in the two resulting approximations is acceptable for all $\ell \le \ell_{\max}$. For a relative difference of three percent, $\ell_{\max} = 62$ for B_ℓ and $\ell_{\max} = 38$ for D_ℓ are sufficient. In this range, the even and odd subsequences $\{B_\ell\}_{\ell=0}^\infty$ and $\{D_\ell\}_{\ell=0}^\infty$ decay monotonically at a fairly constant rate. We use the slightly slower rates given by the odd subsequences: $\mathcal{B}_{17}^{33} = 1.5511$ and $\mathcal{D}_{17}^{33} = 0.7691$ (see Table 4.4). According to (4.4), we expect E_N and R_N to both converge at a rate of $r+1/2$ when the filter is on and to converge at rates q and $r+1/2$,

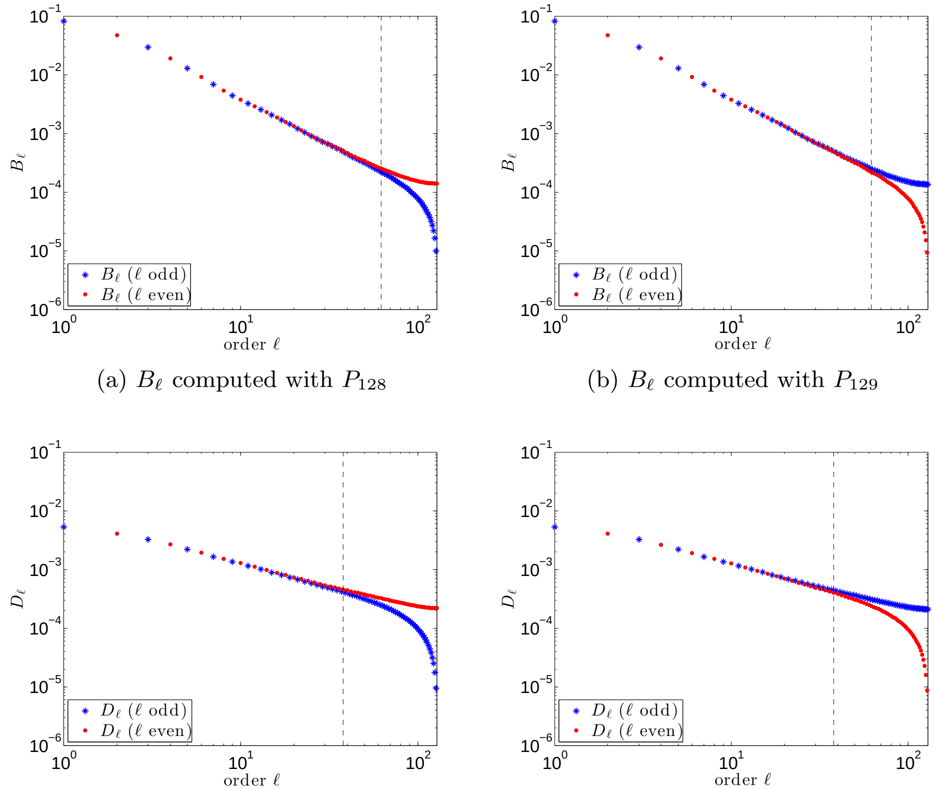

(a) B_ℓ computed with P_{128}

(b) B_ℓ computed with P_{129}

(c) D_ℓ computed with P_{128}

(d) D_ℓ computed with P_{129}

Fig. 4.2: Lattice test: Log-log plot of the sequences B_ℓ and D_ℓ vs. the order ℓ. The dashed lines indicate until which point the relative difference between the sequences computed with P_{128} and P_{129} differs by no more than 3%.

respectively, when the filter is off. Using (4.7), we approximate $q \approx B_{17}^{33} - 1/2 = 1.0511$ and $r + 1/2 \approx D_{17}^{33} = 0.7691$. However from Table 4.5, the convergence rate is roughly one in all cases, meaning that the observed convergence is actually slightly better than any of the estimates that depend on r.

4.3. Hemisphere test. In our final test, we consider a problem with input data that is smooth with respect to the spatial variable but a source term that is discontinuous in the angle variable. As a consequence, we expect that $r = q < \alpha$ so that the convergence order does not depend on α.

The domain is a 1.2×1.2 square centered at the origin with a 300×300 spatial grid (or 150×150 for Table 4.1). The final time is $t = 0.3$. There is no material medium (i.e. $\sigma_{\mathrm{t}} = 0$) and the initial condition is zero everywhere. The source term S is

$$S(t, x, \Omega) = W(x)\chi_{\mathbb{R}^+}(\Omega_1), \tag{4.9}$$

where $W(x) = \frac{1}{4\pi \times 10^{-3}} \exp\left(-\frac{x_1^2 + x_2^2}{4 \times 10^{-3}}\right)$ and $\chi_{\mathbb{R}^+}$ is the characteristic function over

(N_1,N_2)	$B_{N_1}^{N_2}$	$D_{N_1}^{N_2}$
(2,4)	1.3188	0.6213
(4,8)	1.8212	0.8161
(8,16)	1.5208	0.8293
(16,32)	1.5782	0.8679

(a) even order moments

(N_1,N_2)	$B_{N_1}^{N_2}$	$D_{N_1}^{N_2}$
(3,5)	1.6167	0.7818
(5,9)	1.8371	0.8204
(9,17)	1.4901	0.7998
(17,33)	1.5511	0.7691

(b) odd order moments

Table 4.4: Lattice test: Approximate decay rates of the sequence of the moments B_ℓ (and the moments of the differentials D_ℓ). (a) Even order moments $N_2 = 2^{k+1}$ vs. $N_1 = 2^k$ and (b) odd order moments $N_2 = 2^{k+1}+1$ vs. $N_1 = 2^k+1$ with $k = 1,\dots,5$ (Computed with P_{129}).

Filter order	$\mathcal{E}_3^5$	$\mathcal{E}_5^9$	$\mathcal{E}_9^{17}$	$\mathcal{E}_{17}^{33}$	$\mathcal{R}_3^5$	$\mathcal{R}_5^9$	$\mathcal{R}_9^{17}$	$\mathcal{R}_{17}^{33}$
2	0.89	0.80	0.94	1.05	0.86	0.78	0.93	1.05
4	1.02	1.15	1.13	1.05	0.98	1.21	1.21	1.06
8	1.20	1.22	1.04	1.06	1.32	1.55	1.14	1.16
16	1.61	1.31	1.03	1.04	2.10	2.12	1.23	1.20
∞	1.10	0.95	0.98	1.00	1.10	0.85	0.95	0.96

Table 4.5: Lattice Test: Filter order of ∞ means that no filter is applied. The term $\mathcal{E}_{N_1}^{N_2}$ is the convergence rate when going from N_1 to N_2.

$\mathbb{R}^+$. Since S only depends on x and $\Omega_1 = \Omega \cdot e_1$ with $e_1 = (1,0,0)^T$, its expansion in spherical harmonics is

$$S(t,x,\Omega) = W(x)\sum_{\ell=0}^{\infty}\sum_{k=-\ell}^{\ell} s_\ell m_\ell^k(e_1)m_\ell^k(\Omega), \text{ with } s_\ell = 2\pi\int_0^1 P_\ell(\eta)d\eta = 2\pi\frac{P_{\ell-1}(0)-P_{\ell+1}(0)}{2\ell+1}. \tag{4.10}$$

In particular, all the moments with ℓ even are zero.

As before, we determine the smoothness of the exact solution numerically. To this end, we compute P_N solutions which are highly resolved in the angular variable. Again, we observe parity in B_ℓ and D_ℓ with respect to ℓ. However, unlike the lattice problem, the values do not depend on the parity of N_{true}. This fact is confirmed in Figure 4.3, which shows values of B_ℓ and D_ℓ approximated with $N_{\text{true}} = 98$ and $N_{\text{true}} = 99$, respectively. For $\ell = 0,\dots,75$ the values of B_ℓ (as well as D_ℓ) with $N_{\text{true}} = 98$ and $N_{\text{true}} = 99$ coincide up to machine precision. Figure 4.3 also shows that the odd subsequences of B_ℓ and D_ℓ have larger values than the even ones. This can be explained by the form of the source, whose even order moments are identically zero; nonzero values are only generated by spatial gradients of the odd moments. Although the values of the even and odd subsequences differ, the order of the decay rates of the sub-sequences are almost the same in the range $16 \le \ell \le 90$. In particular, (4.7) with $N_1 = 17$ and $N_2 = 33$ (cf. Table 4.6) yields the estimate $q \approx r \approx 1/2$. According to (4.4), the order of the error terms are given by $\min\{q, r+\frac{1}{2}, \alpha\} = q \approx 1/2$, except the order of the unfiltered P_N error term R_N, which is approximately one. These predictions match the observed orders of convergence given in Table 4.7.

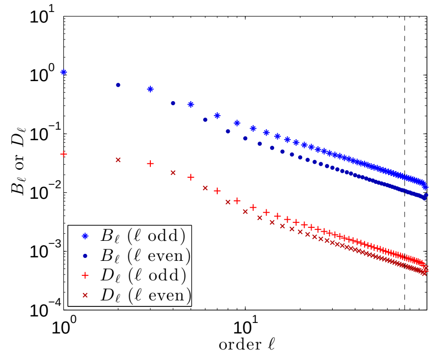

(a) P_{98}

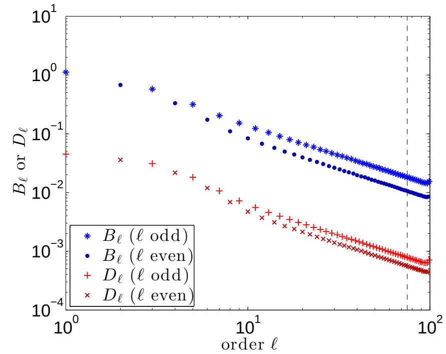

(b) P_{99}

Fig. 4.3: Hemisphere test: Log-log plot of the sequences B_ℓ and D_ℓ against the order ℓ. The dashed lines indicate until which point the sequences computed with P_{98} and P_{99} coincide up to machine precision.

(N_1, N_2)	$B_{N_1}^{N_2}$	$D_{N_1}^{N_2}$
(2,4)	1.0221	0.7133
(4,8)	1.5839	1.6689
(8, 16)	1.1459	1.3454
(16,32)	1.0085	1.0288
(32,64)	0.9963	1.0008

(a) even order moments

(N_1, N_2)	$B_{N_1}^{N_2}$	$D_{N_1}^{N_2}$
(3,5)	1.1774	1.0546
(5,9)	1.2450	1.5673
(9, 17)	1.0202	1.1413
(17,33)	0.9906	1.0076
(33,65)	0.9921	0.9962

(b) odd order moments

Table 4.6: Hemisphere test: Approximated decay rates of the sequence of the moments B_ℓ (and the moments of the differentials D_ℓ). (a) Even order moments $N_2 = 2^{k+1}$ vs. $N_1 = 2^k$ and (b) odd order moments $N_2 = 2^{k+1} + 1$ vs. $N_1 = 2^k + 1$ with $k = 1, \dots, 5$ (Computed with P_{99}).

5. Conclusions. In this paper, we have proven global L^2 convergence properties for filtered spherical harmonic (FP_N) equations. These equations govern the evolution of the coefficients in a spectral approximation, with respect to the angular variable, of a radiative transport equation. The estimates derived here are based on the reformulation of the filter in [34] as an additional anisotropic scattering term in the transport equation which depends on the order of the spectral approximation.

We have shown how the convergence rates depend on both the regularity of the underlying transport solution and the order of the filter. In particular, we observe that for problems with smooth solutions, the order of the filter determines the rate of convergence, while for non-smooth problems, it is the regularity of the transport equation. In addition, we have shown that sharper estimates are possible if the angular L^2 projection of the transport solution onto rotationally invariant subspaces satisfies additional mild conditions. Finally, we have presented numerical convergence results for several test problems which demonstrate various aspects of the theoretical predictions.

Filter order	$\mathcal{E}_3^5$	$\mathcal{E}_5^9$	$\mathcal{E}_9^{17}$	$\mathcal{E}_{17}^{33}$	$\mathcal{R}_3^5$	$\mathcal{R}_5^9$	$\mathcal{R}_9^{17}$	$\mathcal{R}_{17}^{33}$
2	0.55	0.58	0.57	0.58	0.44	0.61	0.59	0.52
4	0.67	0.60	0.55	0.61	0.71	0.70	0.57	0.52
8	0.75	0.61	0.56	0.63	1.06	0.83	0.61	0.56
16	0.77	0.64	0.57	0.64	1.14	1.03	0.79	0.64
∞	0.71	0.59	0.56	0.65	1.33	1.26	0.99	0.96

Table 4.7: Hemisphere test: Filter order of ∞ means that no filter is applied. The term $\mathcal{E}_{N_1}^{N_2}$ is the convergence rate when going from N_1 to N_2.

While most of the results agree with the theoretical predictions, we do observe one discrepancy for the hemisphere test case. There the convergence of the filtered solution is actually slightly better that what is predicted by the estimates on the closure error. Thus, either our estimates are not quite optimal or the numerical simulations used to approximate the decay in the moments of the true transport solution (upon which the estimates depend) are not resolved enough. Further investigation of this issue is ongoing.

Our analysis has been performed using global norms. We can show how a filter has to be chosen so as to not destroy the accuracy of the method. In many examples [27,34] however, it has been observed that filtering drastically improves the quality of the solution near discontinuities. This behavior is not captured by global norms. A local analysis is therefore the scope of future work.

Appendix A. Real-valued P_N equations. We consider the properties of the matrices $\mathbf{A}_i$, which occur in the real-valued P_N equations (2.13)

$$\partial_t \mathbf{u}_{\mathrm{P}_N} + \mathbf{A} \cdot \nabla_x \mathbf{u}_{\mathrm{P}_N} + \sigma_{\mathrm{a}} \mathbf{u}_{\mathrm{FP}_N} - \sigma_{\mathrm{s}} \mathbf{G} \mathbf{u}_{\mathrm{FP}_N} = \mathbf{s}. \tag{A.1}$$

First, we turn our attention to the complex-valued spherical harmonic basis functions, which are analyzed in [8]. They fulfill the following recursion relation:

$$\Omega \overline{Y_\ell^k} = \frac{1}{2} \begin{bmatrix} -c_{\ell-1}^{k-1} \overline{Y_{\ell-1}^{k-1}} + d_{\ell+1}^{k-1} \overline{Y_{\ell+1}^{k-1}} + e_{\ell-1}^{k+1} \overline{Y_{\ell-1}^{k+1}} - f_{\ell+1}^{k+1} \overline{Y_{\ell+1}^{k+1}} \\ i \left(c_{\ell-1}^{k-1} \overline{Y_{\ell-1}^{k-1}} - d_{\ell+1}^{k-1} \overline{Y_{\ell+1}^{k-1}} + e_{\ell-1}^{k+1} \overline{Y_{\ell-1}^{k+1}} - f_{\ell+1}^{k+1} \overline{Y_{\ell+1}^{k+1}} \right) \\ 2 (a_{\ell-1}^k \overline{Y_{\ell-1}^k} + b_{\ell+1}^k \overline{Y_{\ell+1}^k}) \end{bmatrix} , \tag{A.2}$$

where the coefficients are [8]

$$\begin{aligned} a_\ell^k &= \sqrt{\tfrac{(\ell-k+1)(\ell+k+1)}{(2\ell+3)(2\ell+1)}} , \quad & b_\ell^k &= \sqrt{\tfrac{(\ell-k)(\ell+k)}{(2\ell+1)(2\ell-1)}} , \quad & c_\ell^k &= \sqrt{\tfrac{(\ell+k+1)(\ell+k+2)}{(2\ell+3)(2\ell+1)}} , \\ d_\ell^k &= \sqrt{\tfrac{(\ell-k)(\ell-k-1)}{(2\ell+1)(2\ell-1)}} , \quad & e_\ell^k &= \sqrt{\tfrac{(\ell-k+1)(\ell-k+2)}{(2\ell+3)(2\ell+1)}} , \quad & f_\ell^k &= \sqrt{\tfrac{(\ell+k)(\ell+k-1)}{(2\ell+1)(2\ell-1)}} . \end{aligned} \tag{A.3}$$

Note, that for any $\ell = 0, 1, 2 \ldots$ and $-\ell \leq k \leq \ell$ these coefficients satisfy:

$$a_\ell^k = a_\ell^{-k}, \quad b_\ell^k = b_\ell^{-k}, \quad c_\ell^k = e_\ell^{-k}, \quad \text{and} \quad d_\ell^k = f_\ell^{-k}. \tag{A.4}$$

This leads to a similar recursion relation for the real-valued spherical harmonic basis functions, defined in (2.8):

$$\Omega \mathbf{m}_\ell^k = \frac{1}{2} \begin{bmatrix} (1-\delta_{k,-1}) (\tilde{c}_{\ell-1}^{|k|-1} \mathbf{m}_{\ell-1}^{k^-} - \tilde{d}_{\ell+1}^{|k|-1} \mathbf{m}_{\ell+1}^{k^-}) - \tilde{e}_{\ell-1}^{|k|+1} \mathbf{m}_{\ell-1}^{k^+} + \tilde{f}_{\ell+1}^{|k|+1} \mathbf{m}_{\ell+1}^{k^+} \\ \operatorname{sgn}(k) \left((1-\delta_{k,1}) (-\tilde{c}_{\ell-1}^{|k|-1} \mathbf{m}_{\ell-1}^{-k^-} + \tilde{d}_{\ell+1}^{|k|-1} \mathbf{m}_{\ell+1}^{-k^-}) - \tilde{e}_{\ell-1}^{|k|+1} \mathbf{m}_{\ell-1}^{-k^+} + \tilde{f}_{\ell+1}^{|k|+1} \mathbf{m}_{\ell+1}^{-k^+} \right) \\ 2 (a_{\ell-1}^k \mathbf{m}_{\ell-1}^k + b_{\ell+1}^k \mathbf{m}_{\ell+1}^k) \end{bmatrix} , \tag{A.5}$$

where $\delta_{i,j}$ denotes the Kronecker delta, and $\operatorname{sgn}(k)$ denotes the sign function (with abuse of notation in zero: $\operatorname{sgn}(0) \equiv 1$). The coefficients are given by

$$
\begin{aligned}
& k^+ = k + \operatorname{sgn}(k), && k^- = k - \operatorname{sgn}(k) \\
& \tilde{c}_\ell^k = \begin{cases} 0\,, & k<0 \\ \sqrt{2}c_\ell^k\,, & k=0 \\ c_\ell^k\,, & k>0 \end{cases}\,, && \tilde{d}_\ell^k = \begin{cases} 0\,, & k<0 \\ \sqrt{2}d_\ell^k\,, & k=0 \\ d_\ell^k\,, & k>0 \end{cases}\,, \\
& \tilde{e}_\ell^k = \begin{cases} \sqrt{2}e_\ell^k\,, & k=1 \\ e_\ell^k\,, & k>1 \end{cases}\,, && \tilde{f}_\ell^k = \begin{cases} \sqrt{2}f_\ell^k\,, & k=1 \\ f_\ell^k\,, & k>1 \end{cases}\,.
\end{aligned}
\tag{A.6}
$$

The recursion relation is used in (2.10) to obtain the explicit formulation of the P_N equations

$$
\partial_t \mathbf{u}_{\mathrm{P}_N} + \mathbf{A} \cdot \nabla_x \mathbf{u}_{\mathrm{P}_N} + \sigma_{\mathrm{a}} \mathbf{u}_{\mathrm{FP}_N} - \sigma_{\mathrm{s}} \mathbf{G} \mathbf{u}_{\mathrm{FP}_N} = \mathbf{s}, \tag{A.7}
$$

with $\mathbf{A}_i = \langle \mathbf{m}\mathbf{m}^T \Omega_i \rangle$ and $i \in \{x, y, z\}$. Moreover, it shows the existence of the matrices $\mathbf{a}_\ell^{(i)}$ of size $(2\ell-1) \times (2\ell+1)$, which satisfy (2.15)

$$
\mathbf{A}_i = \begin{bmatrix}
0 & \mathbf{a}_1^{(i)} & & & \\
\left(\mathbf{a}_1^{(i)}\right)^T & 0 & \mathbf{a}_2^{(i)} & & \\
& \left(\mathbf{a}_2^{(i)}\right)^T & 0 & \mathbf{a}_3^{(i)} & \\
& & \ddots & \ddots & \ddots \\
& & & \left(\mathbf{a}_{N+1}^{(i)}\right)^T & 0
\end{bmatrix}. \tag{A.8}
$$

The first matrices $\mathbf{a}_\ell^{(i)}$ are given by

$$
\begin{aligned}
&\mathbf{a}_1^{(x)} = \begin{bmatrix} 0 & 0 & \frac{1}{\sqrt{2}} f_1^1 \end{bmatrix}, \mathbf{a}_1^{(y)} = \begin{bmatrix} \frac{1}{\sqrt{2}} f_1^1 & 0 & 0 \end{bmatrix}, \mathbf{a}_1^{(z)} = \begin{bmatrix} 0 & b_1^1 & 0 \end{bmatrix}, \\
&\mathbf{a}_2^{(x)} = \frac{1}{2} \begin{bmatrix} f_2^2 & 0 & 0 & 0 & 0 \\ 0 & 0 & 0 & \sqrt{2} f_2^1 & 0 \\ 0 & 0 & -\sqrt{2} d_2^0 & 0 & f_2^2 \end{bmatrix}, \mathbf{a}_2^{(y)} = \frac{1}{2} \begin{bmatrix} 0 & 0 & -\sqrt{2} d_2^0 & 0 & -f_2^2 \\ 0 & \sqrt{2} f_2^1 & 0 & 0 & 0 \\ f_2^2 & 0 & 0 & 0 & 0 \end{bmatrix}, \\
&\mathbf{a}_2^{(z)} = \begin{bmatrix} 0 & b_2^1 & 0 & 0 & 0 \\ 0 & 0 & b_2^0 & 0 & 0 \\ 0 & 0 & 0 & b_2^1 & 0 \end{bmatrix}, \ldots
\end{aligned}
\tag{A.9}
$$

Since the coefficients $a_\ell^k, \ldots, f_\ell^k$ are bounded by 1, the entries of the matrices $\mathbf{a}_\ell^{(i)}$ are in the interval $[-1, 1]$. Together with the recursion relation (A.5), this yields upper bounds for the ∞-norm and the 1-norm

$$
\|\mathbf{a}_\ell^{(i)}\|_\infty \leq 1 \quad \text{and} \quad \|\mathbf{a}_\ell^{(i)}\|_1 \leq 4 \tag{A.10}
$$

and by implication we also get an estimate for the 2-norm $\|\mathbf{a}_\ell^{(i)}\|_2 \leq \|\mathbf{a}_\ell^{(i)}\|_\infty \|\mathbf{a}_\ell^{(i)}\|_1 \leq 4$. This is used to estimate the closure error in (3.29).

REFERENCES

[1] G. Alldredge, C. D. Hauck, and A. L. Tits, *High-order, entropy-based closures for linear transport in slab geometry II: A computational study of the optimization problem*, SIAM J. Sci. Comput., 34 (2012), pp. B361–B391.

[2] Graham W Alldredge, Cory D Hauck, Dianne P OLeary, and André L Tits, *Adaptive change of basis in entropy-based moment closures for linear kinetic equations*, Journal of Computational Physics, 258 (2014), pp. 489–508.

[3] Kendall Atkinson and Weimin Han, *Spherical harmonics and approximations on the unit sphere: an introduction*, vol. 2044, Springer, 2012.

[4] C. Berthon, M. Frank, C. Sarazin, and R. Turpault, *Numerical methods for balance laws with space dependent flux: Application to radiotherapy dose calculation.*, Communications in Computational Physics, 10 (2011), p. 1184.

[5] John P Boyd, *Chebyshev and Fourier spectral methods*, Courier Dover Publications, 2013.

[6] H. Brezis, *Functional analysis, Sobolev spaces and partial differential equations*, Springer-Verlag, 2011.

[7] T. A. Brunner, *Forms of approximate radiation transport*, Tech. Report SAND2002-1778, Sandia National Laboratories, 2002.

[8] T. A. Brunner and J. P. Holloway, *Two-dimensional time-dependent Riemann solvers for neutron transport*, J. Comp Phys., 210 (2005), pp. 386–399.

[9] C Canuto, MY Hussaini, A Quarteroni, and TA Zang, *Spectral Methods: Fundamentals in Single Domains.*, Springer-Verlag, 2006.

[10] Kenneth M Case and Paul F Zweifel, *Linear transport theory*, vol. 196, Addison-Wesley Reading, Mass., 1967.

[11] J.-F. Coulombel, F. Golse, and T. Goudon, *Diffusion approximation and entropy-based moment closure for kinetic equations*, Asymptotic Analysis, 45 (2005), pp. 1–39.

[12] R. Dautray and J. L. Lions, *Mathematical Analysis And Numerical Methods For Science And Technology, Volume 6: Evolution Problems II*, Spinger-Verlag, Berlin, 2000.

[13] B. Dubroca and J.-L. Fuegas, *Étude théorique et numérique d'une hiérarchie de modèles aux moments pour le transfert radiatif*, C.R. Acad. Sci. Paris, I. 329 (1999), pp. 915–920.

[14] R. Duclous, B. Dubroca, and M. Frank, *A deterministic partial differential equation model for dose calculation in electron radiotherapy*, Physics in medicine and biology, 55 (2010), p. 3843.

[15] C.K. Garrett and C.D. Hauck, *A comparison of moment closures for linear kinetic transport equations: the line source benchmark*, Transp. Theory Stat. Phys., (2014).

[16] Clinton Groth and James McDonald, *Towards physically realizable and hyperbolic moment closures for kinetic theory*, Continuum Mech. Thermodyn., 21 (2009), pp. 467–493.

[17] B. Guo, *Spectral methods and their applications*, World Scientific, 1998.

[18] B. Guo and J. Zheng, *The spectral approximation of barotropic vorticity equations*, Journal of Computational Mathematics, 12 (1994), pp. 173–184.

[19] Cory D. Hauck and Ryan G. McClarren, *Positive P_N closures*, SIAM J. Sci. Comput., 32 (2010), pp. 2603–2626.

[20] Jan Hesthaven and Robert Kirby, *Filtering in legendre spectral methods*, Mathematics of Computation, 77 (2008), pp. 1425–1452.

[21] J. Hesthaven and K. Robert, *Filtering in legendre spectral methods*, Mathematics of Computation, 77 (2008), pp. 1425–1452.

[22] J. S. Hesthaven, S. Gottlieb, and D. Gottlieb, *Spectral methods for time-dependent problems*, vol. 21, Cambridge University Press, 2007.

[23] E. W. Larsen, M. M. Miften, B. A. Fraass, and I. A. D. Bruinvis, *Electron dose calculations using the method of moments*, Med. Phys., 24 (1997), pp. 111–125.

[24] E. E. Lewis and W. F. Miller, *Computational Methods of Neutron Transport*, John Wiley and Sons, 1984.

[25] M. Gonzlez, E. Audit, and P. Huynh, *Heracles: a three-dimensional radiation hydrodynamics code*, Astronomy & Astrophysics, 464 (2007), pp. 429–435.

[26] Daniele L Marchisio and Rodney O Fox, *Computational models for polydisperse particulate and multiphase systems*, Cambridge University Press, 2013.

[27] R.G. McClarren and C.D. Hauck, *Robust and accurate filtered spherical harmonics expansions for radiative transfer*, J. Comput. Phys., 229 (2010), pp. 5597–5614.

[28] Ryan G McClarren and Cory D Hauck, *Simulating radiative transfer with filtered spherical harmonics*, Physics Letters A, 374 (2010), pp. 2290–2296.

[29] Robert McGraw, *Description of aerosol dynamics by the quadrature method of moments*, Aerosol Science and Technology, 27 (1997), pp. 255–265.

[30] G. N. Minerbo, *Maximum entropy Eddington factors*, J. Quant. Spectrosc. Radiat. Transfer, 20 (1978), pp. 541—545.

[31] Claus Müller, *Spherical harmonics*, vol. 17, Springer-Verlag Berlin, 1966.

[32] Ph. Nicolaï, J.-L. Feugeas, C. Regan, M. Olazabal-Loumé, J. Breil, B. Dubroca, J.-P. Morreeuw, and V. Tikhonchuk, *Effect of the plasma-generated magnetic field on relativistic electron transport*, Phys. Rev. E, 84 (2011), p. 016402.

[33] Gerald C. Pomraning, *The Equations of Radiation Hydrodynamics*, Dover Publications, 2005.

[34] D. Radice, E. Abdikamalov, L. Rezzola, and C.D. Ott, *A new spherical harmonics scheme for multi-dimensional radiation transport I: static matter configurations*, J. Comput. Phys., 242 (2013), pp. 648–669.

[35] C. Schmeiser and A. Zwirchmayr, *Convergence of moment methods for linear kinetic equations*, SIAM J. Numer. Anal., 36 (1999), pp. 74–88.

[36] B. Seibold and M. Frank, *Starmap code.* Website. http://www.math.temple.edu/∼seibold/research/starmap.

[37] ———, *StaRMAP - a second order staggered grid method for spherical harmonics moment equations of radiative transfer*, to appear in ACM Trans. Math. Softw., (2014).

[38] Denis Serre, *Systems of Conservation Laws 1: Hyperbolicity, entropies, shock waves*, vol. 1, Cambridge University Press, 1999.

[39] R. Turpault, *A multigroup M1 model for radiation hydrodynamics and applications*, in 23rd internationnal symposium on rarefied gas dynamics, A.D. Ketsdever and E.P. Muntz, eds., American Institute of Physics, 2004.

[40] H. Vandeven, *Family of spectral filters for discontinuous problems*, Journal of Scientific Computing, 6 (1991), pp. 159–192.

[41] V Vikas, CD Hauck, ZJ Wang, and RO Fox, *Radiation transport modeling using extended quadrature method of moments*, Journal of Computational Physics, 246 (2013), pp. 221–241.